Challenge Journal of Structural Mechanics

Research Article

# Numerical investigation of the effective mechanical properties of Octet Truss lattice structures with different strut geometry

Hojjat Ghahramanzadeh Asl [a,*], Elif Altıntaş Kahriman [b,*], Derya Karaman [a]

[a] *Department of Mechanical Engineering, Karadeniz Technical University, 61080 Trabzon, Türkiye*
[b] *Department of Software Engineering, Haliç University, 34060 İstanbul, Türkiye*

**ABSTRACT**

Lattice structures have an important role in lightweight structure applications as they can supply their mechanical performance with less material. Porous structures designed with inspiration from nature, has been used in many industries such as aerospace, automotive, defense industry and biomedical field. In order to continue these advances, studies on various design configurations of porous structure geometries are carried out. This study aimed to increase the usage potential of Octet Truss lattice structures in various sectors. A numerical model is created for 3 variable parameters: strut geometry, porosity, and material type. The effective elastic modulus values are determined based on the principles of Hooke's law for each model. Based on the obtained effective elastic modulus values, it has been concluded that differences in strut geometries, porosities, and material types contribute to 1.27%, 68.85%, and 29.86% of the observed effects, respectively. In order to establish a correlation between these factors, the data is transmitted to the MATLAB software, where equations are generated using the curve fitting approach. A total of nine equations have been generated and the R-square for these equations above 0.99. According to the two desired constant values, the effective elastic modulus can be calculated using these equations without any restrictions.

**ARTICLE INFO**

*Article history:*
Received 4 August 2023
Revised 25 August 2023
Accepted 14 September 2023

*Keywords:*
Lattice structure
Effective elastic modulus
Finite element analysis
Curve fitting method
Strut geometry

## 1. Introduction

Porous structures are great interest today to supply the superior mechanical performance of lightweight structures (Ashby 2013). In addition to the lightness, they can supply the structure requirements by combining mechanical, thermal, and acoustic properties in one structure (Wadley 2006; Suard et al. 2015). Due to its superior properties, it has been adopted in many industrial fields such as automotive, defense, aerospace, and medical sectors (Vasiliev et al. 2012; Tao et al. 2016; Arabnejad et al. 2017). With the developments in additive manufacturing technology, porous structure applications will be encountered more frequently in more industrial areas. Porous structures have repeatable properties by combining random or regular pores into a particular solid structure (Aney et al. 2023). The randomly assembled porous structures are defined as foam structures (Langlois et al. 2018).

Regular porous structures have a wide variety of geometric configurations. For this, two basic geometric configurations are preferred by researchers: beam-based and triply periodic minimal surface (TPMS) (Majeed et al. 2022). TPMS structures are surface-based cell architectures that have surface equations and can be reproduced infinitely in Cartesian space (Al-Ketan et al 2019). Beam-based structures are cell architectures that are formed by combining various numbers of struts at different angles and nodes (Wang et al. 2020).

The positions of the struts in the structure are directly effective in the change of mechanical properties. Especially the number of struts and their positions at certain angles according to the load direction are very important in load bearing. There are lattice structures assembled in

* *Corresponding author*. Tel.: +90-462-377-3149 ; E-mail address: h.kahramanzade@ktu.edu.tr (H. Ghahramanzadeh Asl)
ISSN: 2149-8024 / DOI: https://doi.org/10.20528/cjsmec.2023.04.002

a unit cell at different angles and strut numbers by many researchers: such as Cube (CB), Body-Centered Cubic (BCC), Face-Centered Cubic (FCC), combination of Cube and Face-Centered Cubic (CFCC), combination of Cube and Body-Centered Cubic (CBFCC), Diamond, Octet Truss, Kelvin Rhombic dodecahedron (Zheng et al. 2019; Refai et al. 2020).

With developments in additive manufacturing, various design configurations are realized for existing lattices or new lattice structures. Wang et al., inspired by the hierarchical structures of biological materials, developed a new unit cell configuration design with an internal strut hierarchy (Wang et al. 2022). Meza et al. (2017) modeled the effect of beam geometry on Young's modulus in four beam-based lattice structures (Octet Truss, Cuboctahedron, 3D Kagome, Tetrakaidecahedron) and evaluated them in experimental and numerical analysis. With the proposed analytical model, hollow strut structures are defined as advantageous geometries in terms of mechanical properties. Wang et al. (2021) propose a new hierarchical lattice design by replacing the original straight struts of the face-centered cubic (FCC) lattice with a series of higher-level circular struts. Researchers mainly focus on modeling porous structures that will exhibit the best mechanical performance for the required design space.

In this study, the effects of strut geometry, porosity, and material type on the mechanical properties of lattice structures are investigated in Octet Truss lattice structures. Lattice structures with different porosity (60%, 70%, and 80%) are modeled using circular, hexagonal, and square geometry for the strut geometry. The effective elastic modulus of each structure is determined by the Finite Element Method according to three material properties. The obtained results are transferred to the MATLAB software and different equations are created with the curve fitting method.

## 2. Material and Method

### *2.1. Lattice structure design*

According to the literature, Octet Truss Lattice models are frequently used in porous structures. The high load carrying capacity of the struts, depending on their location, is the main reason for often preferred this structures. In this study, Octet Truss lattice structures were modeled from struts in circle, hexagonal, and square geometries. Unit cells modeled at 60%, 70%, and 80% porosity were shown in Fig. 1. The unit cells were dimensioned as 1×1×1 mm$^3$. Porosity (P) calculation was determined by volume (Lei et al. 2020):

$$P\ (\%) = \frac{V_0 - V}{V_0} \times 100 \tag{1}$$

In Eq. (1), $V_0$ is the total volume of the cubic unit cell, and $V$ is the volume of the solid part in the lattice unit cell. Dimension values of unit cells with struts with different geometries were in Table 1.

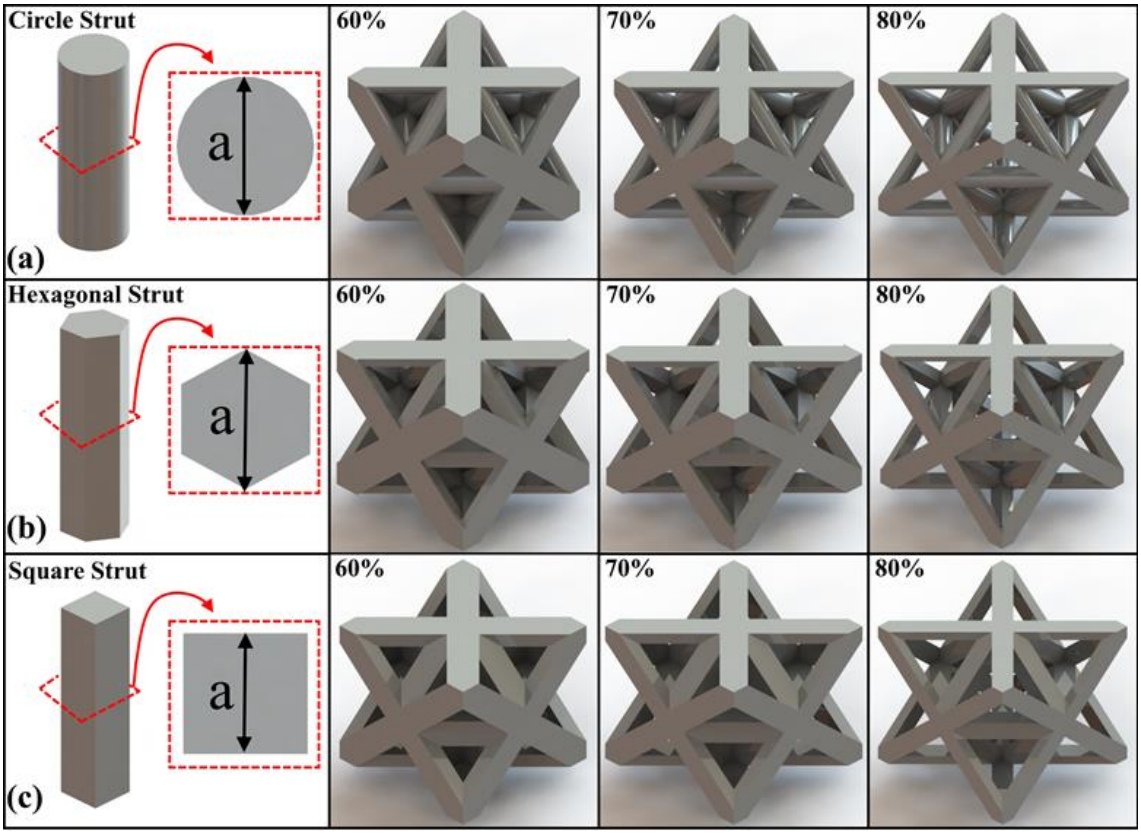


**Fig. 1.** Octet Truss unit cells modeled from struts of different geometry: (a) Circle; (b) Hexagonal; (c) Square.

**Table 1.** Dimension values of unit cells with different geometry struts (a) mm.

| Strut Geometry | Porosity | | |
|---|---|---|---|
| | 60% | 70% | 80% |
| Circle | 0.2071 | 0.1734 | 0.1368 |
| Hexagonal | 0.1973 | 0.1651 | 0.1303 |
| Square | 0.1855 | 0.1550 | 0.1220 |

The porosity value of the unit cells was the ratio of the available lattice structure volume to the cubic volume in a unit. Lattice structures were formed in 5x5x5 array with these unit cells in the x, y, and z directions. The terminology of these lattice structures were included in Table 2. The isometric views of the lattice structures were shown in Fig. 2.

**Table 2.** The terminology of lattice structure.

| Porosity | Strut Geometry | | |
|---|---|---|---|
| | Circle | Hexagonal | Square |
| 60% | OctetT(c)-60 | OctetT(h)-60 | OctetT(s)-60 |
| 70% | OctetT(c)-70 | OctetT(h)-70 | OctetT(s)-70 |
| 80% | OctetT(c)-80 | OctetT(h)-80 | OctetT(s)-80 |

### *2.2. Finite element analysis*

The material types used for the lattice structures were CP-Ti, Ti6Al4V and Stainless Steel 316L, which are commonly used in additive manufacturing technology. The mechanical properties of the materials were listed in Table 3.

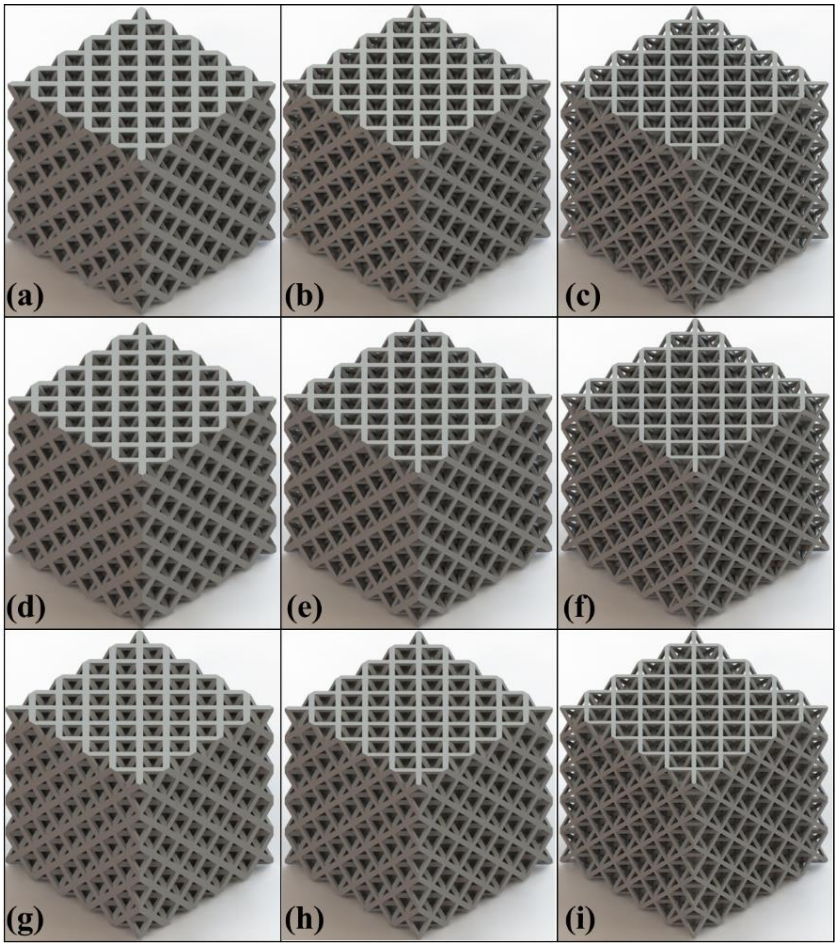


**Fig. 2.** Lattice structures in 5x5x5 array: (a) OctetT(c)-60; (b) OctetT(c)-70; (c) OctetT(c)-80; (d) OctetT(h)-60; (e) OctetT(h)-70; (f) OctetT(h)-80; (g) OctetT(s)-60; (h) OctetT(s)-70; (i) OctetT(s)-80.

**Table 3.** Mechanical properties of materials (Ma et al. 2020; Xu et al. 2019; Mercer et al. 2022).

| Material | Elastic Module (GPa) | Poisson Ratio |
|---|---|---|
| CP-Ti | 108.21 | 0.34 |
| Ti6Al4V | 110 | 0.33 |
| Stainless Steel 316L | 200 | 0.30 |
| Tungsten Carbide (plate material) | 600 | 0.21 |

Compression loads were applied to evaluate the mechanical properties of lattice structures. Finite element analysis method was used to determine the mechanical properties of lattice structures. Accordingly, all lattice structures were analyzed by compression load simulation using ANSYS Workbench software. As a result of these analyses, the effective elastic modulus ($E_{eff}$) values of each lattice structure were calculated according to Hooke's law. In Hooke's law (Eq. (2)):

$$\sigma = E \times \varepsilon$$

$$\varepsilon = \frac{\Delta L}{L_0}$$

$$E_{eff} = \left(\frac{\sigma}{\varepsilon}\right) = \frac{(\sigma \times L_0)}{\Delta L} \quad (2)$$

In Eq. (2), $\sigma$, $L_0$, and $\Delta L$ are the applied normal stress (MPa), the initial length of the model (mm), and directional deformation (mm), respectively.

Plates were placed at the top and bottom of each lattice structure for these simulations. The contact type between the plate and lattice structures was chosen as bonded for all simulations. The bottom plate was defined to be fixed in the *x*, *y*, and *z* directions. The top plate is fixed in the x and z directions and movable in the y direction. Plate geometry was designed as 5x5x1 mm. For the plates, the type of material with higher mechanical strength than the defined material was selected. A normal stress value of 1 MPa in the -*y* direction was defined for the loading conditions (Fig. 3).

Tetrahedral elements of 0.12 mm were used for the mesh size. In the mesh convergence studies, there was no significant change in mesh sizes below 0.12 mm. Therefore, the same mesh size was used for the lattice structures. Mesh convergence analyses were carried out to achieve more stable results for beam connections and surfaces in scaffold designs where stress would be concentrated. Tetrahedral elements were used to create the mesh. The mesh quality indicated a value of 0.8784, accompanied by a standard deviation of 0.9750. Additionally, the skewness of the mesh was measured to be 0.2136, with a standard deviation of 0.1168. Fig. 4 shows the mesh structure of the lattice structures for each strut geometry.

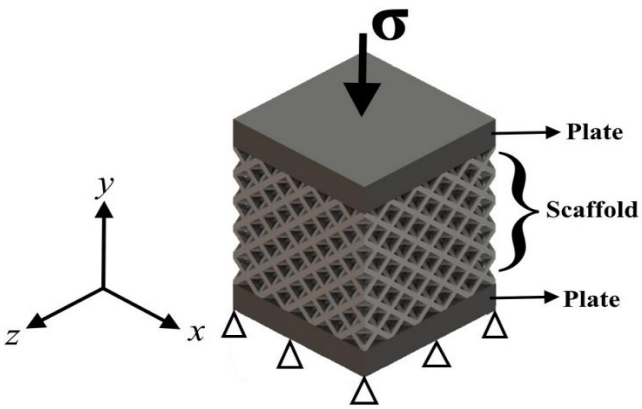


**Fig. 3.** Loading and boundary conditions of lattice structures.

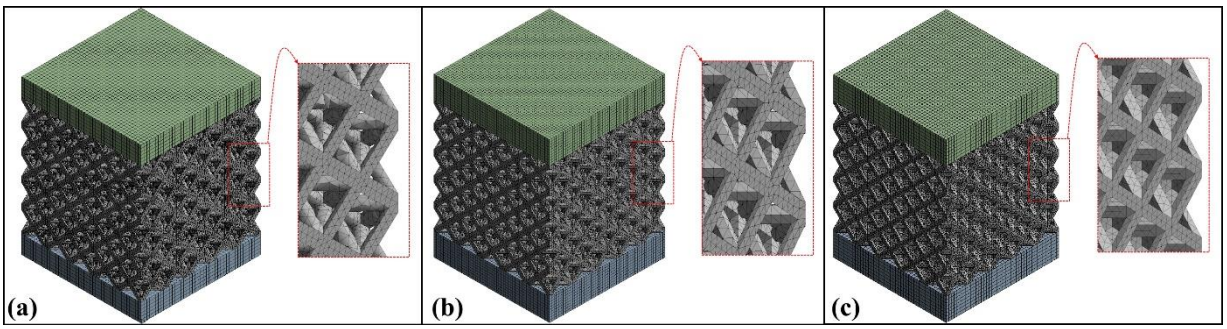


**Fig. 4.** Mesh structures of lattice structures with 70% porosity: (a) Circle; (b) Hexagonal; (c) Square strut geometry.

### *2.3. Statistical analysis*

The Statistical analysis was used to determine the degree of influence of the three parameters (strut geometry, porosity, and material properties) on the effective elastic modulus of Octet Truss lattice structures. The statistical methodology used to investigate the observed differences was the one-way analysis of variance (ANOVA). $p<0.05$ was considered as a statistically significant difference. In this analysis, the signal value ($S$) is the value to be measured, and the noise value ($N$) is the effectiveness of the undesired factors within the measured value. The graphs of the calculated $S/N$ ratios represent the degree of influence of any variable parameter used in the analysis. In addition to the $S/N$ ratio, ANOVA analysis was used to determine the significance levels of variable parameters affecting the mechanical properties of the structures. This analysis was performed with Minitab software.

### *2.4. Curve fitting application*

Curve fitting is a machine learning approach that is often used in the field of data science. It was used to find the optimum fit by investigating the correlation between the dependent and independent variables. The points in the dataset were also utilized to create a curve-shaped linear or nonlinear mathematical function. The statistical correlations used for the data analysis are the sum of squared errors (*SSE*), R-squared ($R^2$), adjusted Rsquare, and root mean square error (*RMSE*). The RMSE approach was used in the following equation (Eq. (3)) to define the error:

$$RMSE = \sqrt{\frac{\sum_{i=1}^{N}(\widehat{y_i} - y_i)^2}{N}} \quad (3)$$

where $N$ is the total number of training data, $y_i$ is the data value at time $t_i$, $\widehat{y_i}$ is the predicted value at time $t_i$.

The following equation was used to determine the error value.

$$\text{Error Value} = \frac{(\text{Actual Value} - \text{Value Obtained by Curve Fitting})}{\text{Actual Value}}\ x\ 100 \quad (4)$$

In this study, (*X*, *Y*, and *Z*) were used as input factors. The data from each lattice structure model for all materials and porosities were analyzed using MATLAB software. For each type of lattice structure, the initial curve fittings were developed. These curve fittings utilized of the material's elastic modulus for the *X* value (108210, 110000, and 200000), the porosity for the *Y* value (60, 70, and 80), and the measured effective elastic modulus for the *Z* value. The second curve fittings were obtained while taking the materials into account; in this case, the lattice structure types (Octet Truss-Circle (1), Octet Truss-Hexagonal (2), and Octet Truss-Square (3)) were taken into account as "*x*," "*y*" values are porosity rates (60, 70, and 80), and "*z*" values are effective elastic modulus values. The third curve fittings took porosity into account. Therefore, "*x*" parameter represented different types of lattice structures (1, 2, and 3), "*y*" values represented different elastic modulus (108210, 110000, and 200000), and "*z*" values represented measurements of the effective elastic modulus values. Additionally, these models' functions were constructed in the MATLAB programming language as 2nd order polynomials.

## 3. Results and Discussions

Compression loads for three types of materials were simulated for Octet Truss lattice structures in different strut geometries and different porosity. The maximum von-Mises stress values obtained by finite element analysis were listed in Table 4. Stress values increased with increasing porosity for each geometry type.

For same material type in Octet Truss lattice structure, strut geometry was an effect on stress generation. At the same porosity ratios, the lowest stress occurred in square geometries, and the highest stress value occurred in hexagonal geometry lattice structure. Considering the effect of strut geometry for Cp-Ti material: There was 27.54% difference between OctetT(s)-60 and OctetT(c)-60, and 18.78% difference between OctetT(c)-60 and OctetT(h)-60 for 60% porosity. There was 23.55% difference between OctetT(s)-70 and OctetT(c)-70, and 20.31% difference between OctetT(c)-70 and OctetT(h)-70 for 70% porosity. There was 4.75% difference between OctetT(s)-80 and OctetT(c)-80, and 20.08% difference between OctetT(c)-80 and OctetT(h)-80 for 80% porosity. This difference situation was similar for other material types. The maximum stress values in lattice structures with the same porosity changed according to the material type. There was not significant difference between CP-Ti and Ti6Al4V materials. This was related to the mechanical properties of these materials close to each other. Lattice structures with 316L steel material had relatively lower stresses compared to other materials. This was due to the high elastic modulus of this material. The distribution contours of these stress values on the lattice structures were shown in Fig. 5.

In Octet Truss lattice structures with the same porosity, the directional deformation value was affected by the strut geometry. Directional deformation occurring in lattice structures with the same porosity was lowest in square geometries and highest in circle geometries. Considering the effect of strut geometry for Ti6Al4V material: There was 12.26% difference between OctetT(s)-60 and OctetT(h)-60, and 4.29% difference between OctetT(h)-60 and OctetT(c)-60 for 60% porosity. There was 8.69% difference between OctetT(s)-70 and OctetT(h)-70, and 5.75% difference between OctetT(h)-70 and OctetT(c)-70 for 70% porosity. There was 8.61% difference between OctetT(s)-80 and OctetT(h)-80, and 5.96% difference between OctetT(h)-80 and OctetT(c)-80 for 80% porosity. These difference ratios could be considered the same for other materials. Considering the material effect on directional deformation, a difference of approximately ~2% was detected for the same porosity ratios for CP-Ti and Ti6Al4V materials. However, when these two material types are compared with the 316L material, the difference value has increased. So, the approximate difference between 316L lattice structures and lattice structures with the same porosity as CP-Ti or Ti6Al4V material was ~85%. The distribution contours of the directional deformations in the lattice structures were shown in Fig. 6.

At the same time, directional deformation (*-y*) values of each lattice structure were recorded by the finite element analysis (Table 5). The occurrence of directional deformation increased with increase porosity.

**Table 4.** von-Mises stresses in lattice structures according to material type (MPa).

| Lattice structure | CP-Ti | Ti6Al4V | 316L |
|---|---|---|---|
| OctetT(c)-60 | 16.795 | 16.759 | 16.678 |
| OctetT(c)-70 | 25.998 | 25.959 | 25.911 |
| OctetT(c)-80 | 43.327 | 43.314 | 44.212 |
| OctetT(h)-60 | 19.949 | 19.994 | 20.085 |
| OctetT(h)-70 | 31.278 | 31.277 | 31.269 |
| OctetT(h)-80 | 52.027 | 52.383 | 53.679 |
| OctetT(s)-60 | 13.168 | 13.155 | 13.109 |
| OctetT(s)-70 | 21.042 | 21.025 | 21.025 |
| OctetT(s)-80 | 41.364 | 41.692 | 42.957 |

**Table 5.** Directional deformation in lattice structures according to material type (mm).

| Lattice structure | CP-Ti | Ti6Al4V | 316L |
|---|---|---|---|
| OctetT(c)-60 | 393.75 E-6 | 387.76 E-6 | 208.54 E-6 |
| OctetT(c)-70 | 647.98 E-6 | 638.10 E-6 | 344.81 E-6 |
| OctetT(c)-80 | 1182.80 E-6 | 1164.70 E-6 | 631.77 E-6 |
| OctetT(h)-60 | 377.42 E-6 | 371.80 E-6 | 201.05 E-6 |
| OctetT(h)-70 | 612.59 E-6 | 603.42 E-6 | 327.41 E-6 |
| OctetT(h)-80 | 1116.10 E-6 | 1099.20 E-6 | 596.96 E-6 |
| OctetT(s)-60 | 336.42 E-6 | 331.20 E-6 | 178.31 E-6 |
| OctetT(s)-70 | 563.94 E-6 | 555.19 E-6 | 300.24 E-6 |
| OctetT(s)-80 | 393.75 E-6 | 387.76 E-6 | 208.54 E-6 |

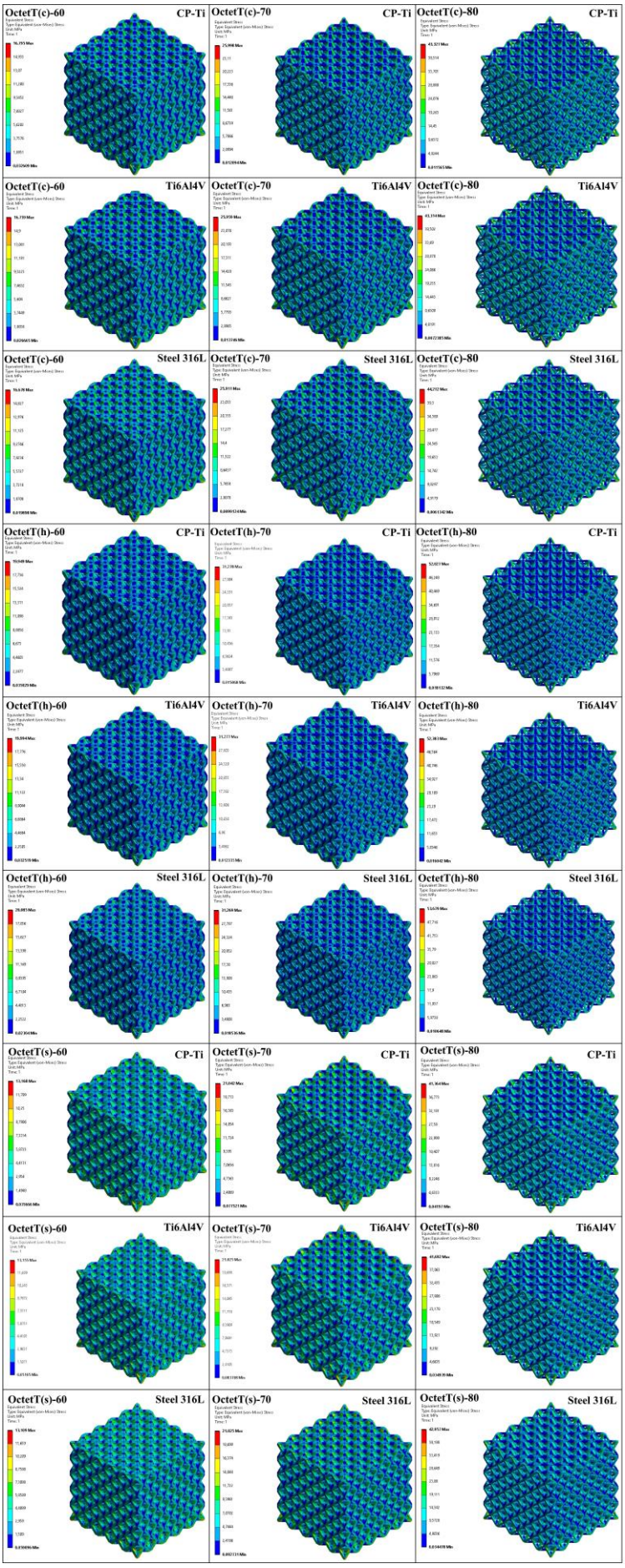


**Fig. 5.** Distribution contours of these von-Mises stress values on the lattice structures.

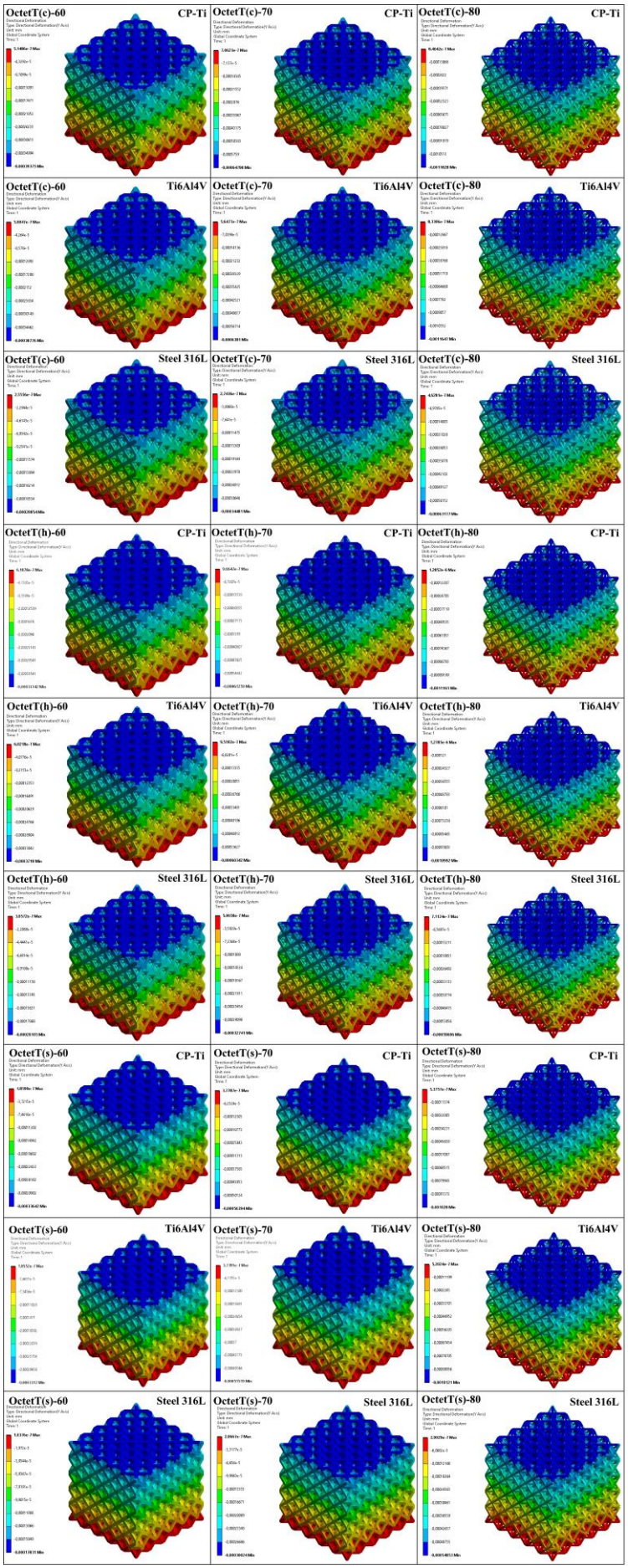


**Fig. 6.** Distribution contours of these directional deformation values on the lattice structures.

The effective elastic modulus of the lattice structure was calculated according to Hooke's law. Calculations were performed according to the directional deformation values listed in Table 5. The graphs of the effective elastic modulus of the lattice structures grouped by material type were shown in Fig. 7. Lattice structures with CP-Ti and Ti6Al4V materials had effective elastic modulus close to each other. Among lattice structures of the same strut geometry and porosity, Ti614V lattice structures had as much as 1.5% greater elasticity than CP-Ti. 316L stainless Steel lattice structures had the highest effective elastic modulus in this material group. Compared to Cp-Ti and Ti6Al4V lattice structures, it had approximately 85% more elastic modulus. This was due to the lattice structures were inversely proportional to the directional deformation. According to the deformations listed in Table 5, the lowest values belonged to the lattice structures with 316L material. This was a clear indication that the mechanical properties of the materials were an influential parameter for mechanical performance in porous structures.

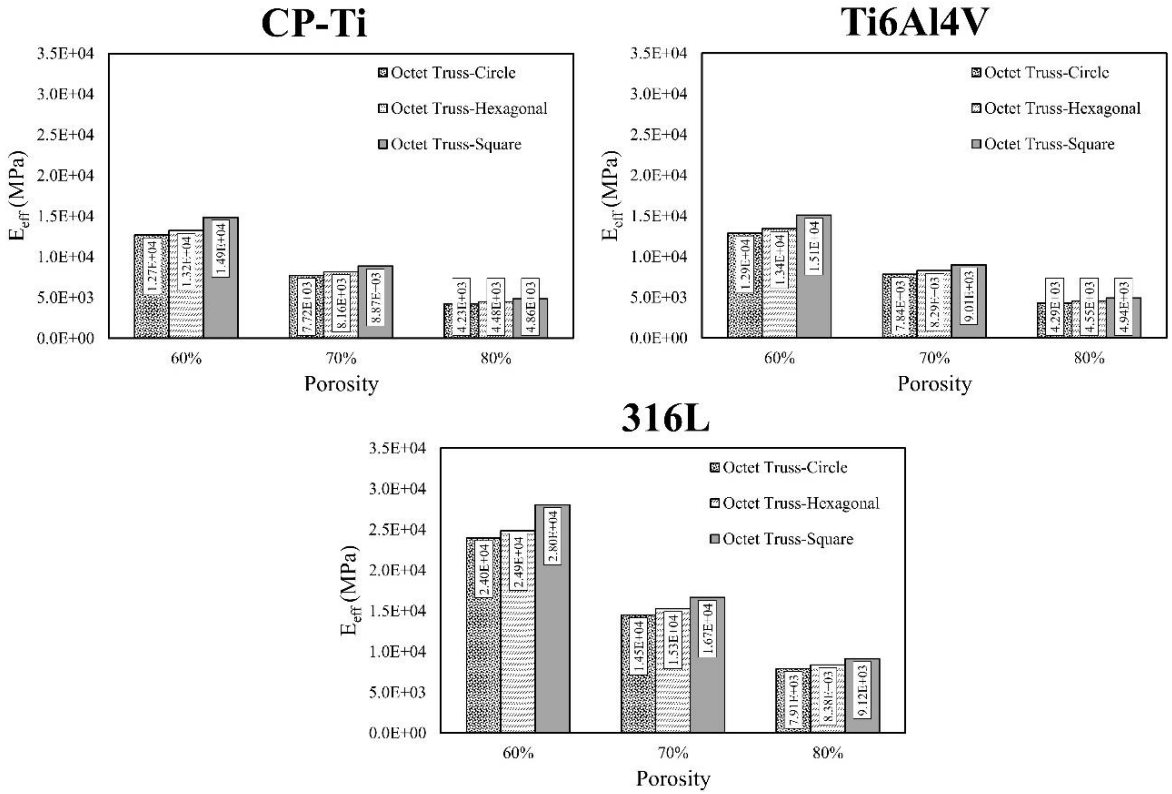


**Fig. 7.** Effective elastic modulus of Octet Truss lattice structures with different strut geometry, determined by material type.

As the porosity of the lattice structures increased, a decrease was observed in the mechanical behavior due to the reduced cross-sectional area of the structures (Maskery et al. 2018). This was known with the results of experimental and numerical analyzes applied in studies (Günther et al. 2022; Park et al. 2022; Bai et al. 2020). Load-bearing areas decreased as porosity increased and structural volume decreased (Zao et al. 2018). This was clearly seen in Octet Truss lattice structures in different geometries. The effective elastic modulus decreased for each type of strut geometry with increasing porosity from 60% to 80%. This decrease occurred at approximately the same rates for each strut geometry. A reduction of approximately ~39% compared to 60% lattice structures at 70%, and approximately ~45% reduction at 80% compared to 70% lattice structures was determined.

It was noted that the strut geometry is an effective parameter for the effective elastic modulus. So, the values with the same porosity for a material type were confirmation of this. The effective elastic modulus value of the lattice structures with the same porosity ratios was the lowest in the circle geometry and the highest in the square geometry. The different values caused by the strut geometries had approximately the same rate of variation for the three material types. Considering the effect of strut geometry for 316L material: There was an increase 3.73% between OctetT(c)-60 and OctetT(h)-60, and an increase 12.75% between OctetT(h)-60 and OctetT(s)-60 for 60% porosity. There was an increase 5.31% between OctetT(c)-70 and OctetT(h)-70, and an increase 9.05% between OctetT(h)-70 and OctetT(s)-70 for 70% porosity. There was an increase 5.83% between OctetT(c)-80 and OctetT(h)-80, and an increase 8.83% between OctetT(h)-80 and OctetT(s)-80 for 80% porosity.

As it could be understood from the results obtained by numerical analysis, the strut geometry, porosity, and material type parameters affected the mechanical performance of the lattice structures at different rates. Statistical analysis results were given in Fig. 8 to understand the degree of influence of the three parameters. A

residual error of 0.02% was found in generating the $S/N$ ratio charts. For Octet Truss lattice structures, strut geometry, porosity and material type parameters had 1.27%, 68.85% and 29.86% effects on the mechanical performances of the lattice structures, respectively. In this statement, the signal value ($S$) is the value to be measured, and the noise value ($N$) is the effectiveness of the undesired factors within the measured value. The graphs of the calculated $S/N$ ratios represent the degree of influence of any variable parameter used in the analysis. In addition to the $S/N$ ratio, ANOVA analysis was used to determine the significance levels of variable parameters affecting the mechanical properties of the structures. This analysis was performed with Minitab software.

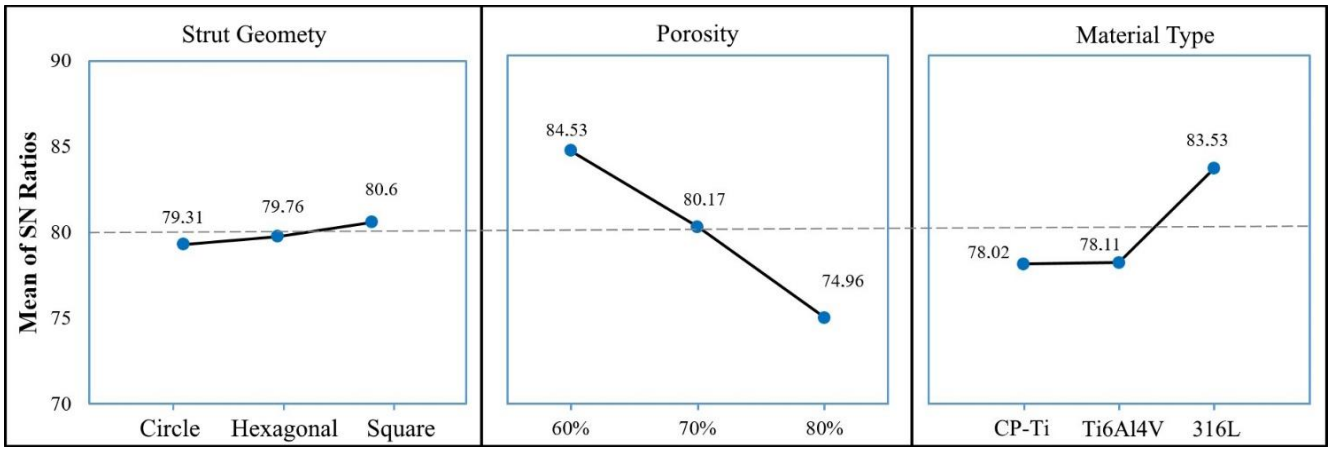


**Fig. 8.** Effect of strut geometry, porosity and material type parameters on effective elastic modulus for Octet Truss lattice structures.

The effective elastic modulus values were inputted into the MATLAB program in order to create a correlation between results. The equations for each lattice structure were generated using the curve fitting technique in the MATLAB program, considering consideration of all materials and porosities. The following equations and R squared values for each lattice structures were shown in Table 6 when the "$x$" value is taken as the elastic modulus of materials (MPa) and the "$y$" value is taken as porosity rates (%). These curve fitting findings were represented graphically in Fig. 9. Table 6 provides equations that are used to calculate the effective elastic modulus of lattice structures depending on the material's elastic modulus value and the desired amount of porosity.

**Table 6.** Curve fitting analysis results in terms of lattice structure type.

| Lattice structure type | Curve fitting equation | R-square |
|---|---|---|
| Octet Truss-Circle | $f_1(x,y,z) = (4.736\,E+4) + 0.3415\,x + (-1351)\;y + (8.857\,E-8)\,x^2 + (-0.00414)\;x\,y + 9.83\,y^2$ | 0.9993 |
| Octet Truss-Hexagonal | $f_2(x,y,z) = (4.518\,E+4) + 0.3465\,x + (-1272)\;y + (9.949\,E-8)\,x^2 + (-0.004214)\;x\,y + 9.218\,y^2$ | 0.9994 |
| Octet Truss-Square | $f_3(x,y,z) = (6.296\,E+4) + 0.4059\,x + (-1809)\;y + (8.561\,E-8)\,x^2 + (-0.004867)\;x\,y + 13.11\,y^2$ | 0.9991 |

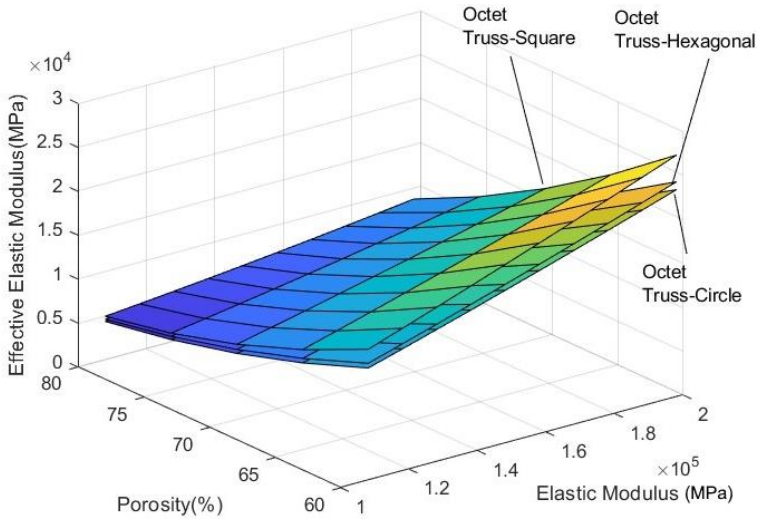


**Fig. 9.** The graphics of curve fitting results for each lattice structure models.

Equations were developed for the second analysis based on the elastic modulus of each material. For each material, "$x$" and "$y$" variables representing lattice structure types and porosities were accepted in these studies. Table 7 provides the curve-fitting formulae and R-squared values in accordance with the results. Additionally, graphs invented of MATLAB curve fitting formulae for each material attribute were provided in Fig. 10. With the lattice structure type and the desired amount of porosity entered into the formulae found in Table 7, it will be feasible to determine how much effective elastic modulus lattice structures will possess.

**Table 7.** Curve fitting analysis results in terms of material properties.

| Elastic modulus of materials | Curve fitting equation | R-square |
|---|---|---|
| 316L | $g_1(x,y,z) = (1.419\,E+5) + 4136\,x + (-2918)\;y + 528\,x^2 + (-71.6)\;x\,y + 15.74\,y^2$ | 0.9989 |
| CP-Ti | $g_2(x,y,z) = (7.411\,E+4) + 2362\,x + (-1519)\;y + 242.5\,x^2 + (-38.19)\;x\,y + 8.151\,y^2$ | 0.9991 |
| Ti6A14V | $g_3(x,y,z) = (7.525\,E+4) + 2391\,x + (-1542)\;y + 250\,x^2 + (-38.87)\;x\,y + 8.276\,y^2$ | 0.9991 |

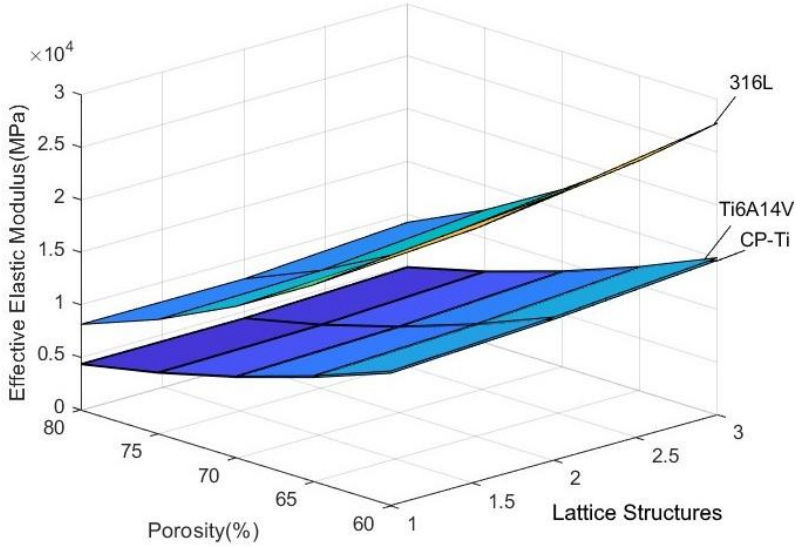


**Fig. 10.** The graphics of curve fitting results for each material properties.

In the end, the "$x$" and "$y$" parameters represent the various types of lattice structures and the elastic modulus of materials, respectively. As a result, each porosity's results were investigated independently. The curve fitting equations and R-squared values for each porosity were provided in Table 8 below. Additionally, the graphs obtained by these curve-fitting equations were shown in Fig. 11. By choose the lattice structure type and the elastic modulus of the material to be design according to the equations in Table 7, the effective elastic modulus values of the lattice structure will be determined.

**Table 8.** Curve fitting analysis results in terms of porosities.

| Porosity | Curve fitting equation | R-square |
|---|---|---|
| 60% | $h_1(x,y,z) = 5232 + (-2997)\,x + 0.06382\,y + 739.8\,x^2 + 0.01035\,x\,y + (1.508\,E-08)\,y^2$ | 0.9994 |
| 70% | $h_2(x,y,z) = 2164 + (-775.1)\,x + 0.04259\,y + 189.9\,x^2 + 0.00546\,x\,y + (18.184\,E-08)\,y^2$ | 0.9998 |
| 80% | $h_2(x,y,z) = 1092 + (-377.9)\,x + 0.0242\,y + 90.83\,x^2 + 0.003075\,x\,y + (4.097\,E-08)\,y^2$ | 0.9999 |

Tables 6, 7, and 8 show that the equations have R-square values of more than 0.99. The term with a low degree of effect compared to the others could be removed from these equations. So that results could be obtained with simpler equations. Since this affects the $R^2$ values of the equations, the equations presented in the study were given with all the details. These figures show that the data used to create the graphs was sufficiently similar to each other. This finding was supported by a closer look at the current study's reaction surface plots (Karaman et al. 2022). These investigations also provide researchers with a reliable mathematical model to estimate these parameters of the input and output for any response value before executing actual tests.

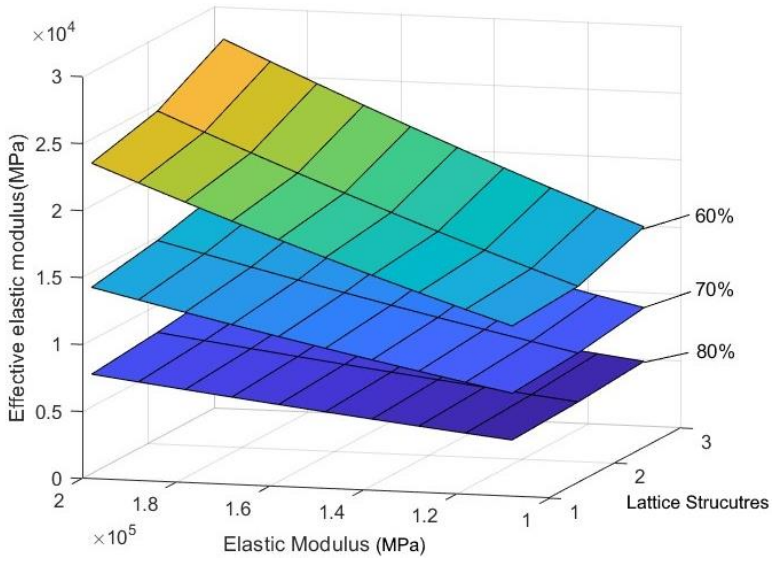


**Fig. 11.** The graphics of curve fitting results for each porosity.

## 4. Conclusions

In this study, the effects of strut geometry, porosity, and material type on the mechanical performance of lattice structures were numerically investigated. The porosities of circular, hexagonal, and square Octet Truss lattice structures were modeled at 60%, 70%, and 80%, respectively. A total of 27 numerical analyzes were performed with three different material types. As a result of the analyses, the effective elastic modulus of the lattice structures were determined according to Hooke's law. It was determined by ANOVA analysis that the strut geometry, porosity and material type parameters had 1.27%, 68.85% and 29.86% effects on the mechanical performances of the lattice structures, respectively. In accordance with the curve fitting technique used for the data produced by finite element analysis, three kinds of polynomial 2nd-order curve equations were developed. A total of nine equations were found, and their R-square values exceeded 0.99. Using two desirable constant values and the nine equations that were found, the effective elastic modulus could be determined. For the engineering industries, especially in the biomedical engineering application, the accuracy of the correlations found for each curve equation was satisfactory. Since there are several options for the geometric and mechanical characteristics of the structure, these curve equations are a reliable tool in design and manufacture planning for a quick manufacturing process.

***Author Contributions***

*All of the authors made substantial contributions to conception and design, or acquisition of data, or analysis and interpretation of data; were involved in drafting the manuscript or revising it critically for important intellectual content; and gave final approval of the version to be published.*

***Acknowledgements***

*None declared.*

***Funding***

*The authors received no financial support for the research, authorship, and/or publication of this manuscript.*

***Conflict of Interest***

*The authors declared no potential conflicts of interest with respect to the research, authorship, and/or publication of this manuscript.*

***Data Availability***

*The datasets created and/or analyzed during the current study are not publicly available, but are available from the corresponding author upon reasonable request.*

## REFERENCES

Al-Ketan O, Abu Al-Rub RK (2019). Multifunctional mechanical metamaterials based on triply periodic minimal surface lattices. *Advanced Engineering Materials*, 21(10), 1900524.

Aney S, & Rege A (2023). The effect of pore sizes on the elastic behaviour of open-porous cellular materials. *Mathematics and Mechanics of Solids*, 28(7), 1624-1634.

Arabnejad S, Johnston B, Tanzer M, Pasini D (2017). Fully porous 3D printed titanium femoral stem to reduce stress-shielding following total hip arthroplasty. *Journal of Orthopaedic Research*, 35(8), 1774-1783.

Ashby M (2013). Designing architectured materials. *Scripta Materialia*, 68(1), 4-7.

Bai L, Gong C, Chen X, Sun Y, Xin L, Pu H, Luo J (2020). Mechanical properties and energy absorption capabilities of functionally graded lattice structures: Experiments and simulations. *International Journal of Mechanical Sciences*, 182, 105735.

Günther F, Wagner M, Pilz S, Gebert A, Zimmermann M (2022). Design procedure for triply periodic minimal surface based biomimetic scaffolds. *Journal of the Mechanical Behavior of Biomedical Materials*, 126, 104871.

Karaman D, Ghahramanzadeh Asl H, Altıntaş Kahriman E (2022). Estimation and Comparison of Effective Elastic Modulus of Different Scaffolds Using Curve Fitting Method for Additive Manufacturing Field. *Arabian Journal for Science and Engineering*, 47, 15973-15987.

Langlois V, Trinh VH, Lusso C, Perrot C, Chateau X, Khidas Y, Pitois O (2018). Permeability of solid foam: Effect of pore connections. *Physical Review E*, 97(5), 053111.

Lei HY, Li JR, Xu ZJ, Wang QH (2020). Parametric design of Voronoi-based lattice porous structures. *Materials & Design*, 191, 108607.

Ma TH, Chang L, Guo S, Kong LR, He XH, Zhou CY (2020). Comparison of multiaxial low cycle fatigue behavior of CP-Ti under strain-controlled mode at different multiaxial strain ratios. *International Journal of Fatigue*, 140, 105818.

Majeed M, Khan HM, Wheatley G, Situ R (2022). Influence of post-processing on additively manufactured lattice structures. *Journal of the Brazilian Society of Mechanical Sciences and Engineering*, 44(9), 389.

Maskery I, Sturm L, Aremu AO, Panesar A, Williams CB, Tuck CJ, Hague RJ (2018). Insights into the mechanical properties of several triply periodic minimal surface lattice structures made by polymer additive manufacturing. *Polymer*, 152, 62-71.

Mercer C, Speck T, Lee J, Balint DS, Thielen M (2022). Effects of geometry and boundary constraint on the stiffness and negative Poisson's ratio behaviour of auxetic metamaterials under quasi-static and impact loading. *International Journal of Impact Engineering*, 169, 104315.

Meza LR, Phlipot GP, Portela CM, Maggi A, Montemayor LC, Comella A, Greer JR (2017). Reexamining the mechanical property space of three-dimensional lattice architectures. *Acta Materialia*, 140, 424-432.

Park SJ, Lee JH, Yang J, Heogh W, Kang D, Yeon SM, Park J (2022). Lightweight injection mold using additively manufactured Ti-6Al-4V lattice structures. *Journal of Manufacturing Processes*, 79, 759-766.

Refai K, Montemurro M, Brugger C, Saintier N (2020). Determination of the effective elastic properties of titanium lattice structures. *Mechanics of Advanced Materials and Structures*, 27(23), 1966-1982.

Suard M, Martin G, Lhuissier P, Dendievel R, Vignat F, Blandin JJ, Villeneuve F (2015). Mechanical equivalent diameter of single struts for the stiffness prediction of lattice structures produced by Electron Beam Melting. *Additive Manufacturing*, 8, 124-131.

Tao W, Leu MC (2016). Design of lattice structure for additive manufacturing. *In 2016 International Symposium on Flexible Automation,* USA, 325-332.

Vasiliev VV, Barynin VA, Razin AF (2012). Anisogrid composite lattice structures–Development and aerospace applications. *Composite structures*, 94(3), 1117-1127.

Wadley HN (2006). Multifunctional periodic cellular metals. Philosophical Transactions of the Royal Society A: Mathematical. *Physical and Engineering Sciences*, 364(1838), 31-68.

Wang P, Bian Y, Yang F, Fan H, Zheng B (2020). Mechanical properties and energy absorption of FCC lattice structures with different orientation angles. *Acta Mechanica*, 231, 3129-3144.

Wang P, Yang F, Ru D, Zheng B, Fan H (2021). Additive-manufactured hierarchical multi-circular lattice structures for energy absorption application. *Materials & Design*, 210, 110116.

Wang M, Zhang J, Wang W, Gao L (2022). Compression behaviors of the bio-inspired hierarchical lattice structure with improved mechanical properties and energy absorption capacity. *Journal of Materials Research and Technology*, 17, 2755-2771.

Xu Y, Zhang D, Hu S, Chen R, Gu Y, Kong X, Jiang Y (2019). Mechanical properties tailoring of topology optimized and selective laser melting fabricated Ti6Al4V lattice structure. *Journal of the mechanical behavior of biomedical materials*, 99, 225-239.

Zhao M, Liu F, Fu G, Zhang DZ, Zhang T, Zhou H (2018). Improved mechanical properties and energy absorption of BCC lattice structures with triply periodic minimal surfaces fabricated by SLM. *Materials*, 11(12), 2411.

Zheng HD, Liu LL, Deng CL, Shi ZF, Ning CY (2019). Mechanical properties of AM Ti6Al4V porous scaffolds with various cell structures. *Rare Metals*, 38, 561-570.